DOI: 10.1002/chem.201000332

Solution-Processable Flower-Shaped Hierarchical Structures: Self-Assembly, Formation, and State Transition of Biomimetic Superhydrophobic Surfaces

Jie Yin,[a] Jing Yan,[a] Min He,[b] Yanlin Song,*[b] Xiaoguang Xu,[a] Kai Wu,*[a] and Jian Pei*[a]

Abstract: Superhydrophobic surfaces inspired by biological microstructures attract considerable attention from researchers because of their potential applications. In this contribution, two kinds of microscale flower-shaped morphologies with nanometer petals formed from the hierarchical self-assembly of benzothiophene derivatives bearing long alkyl chains have been developed as superhydrophobic surfaces. The intermediate stages of the assemblies demonstrated a new formation mechanism for such flower-shaped morphologies. The hierarchical morphologies of the film exhibited excellent water-repelling characteristics as superhydrophobic surfaces, which were prepared by means of a simple solution process. The transition process from the Cassie state to Wenzel state was easily realized owing to the slight microstructural differences in the two kinds of flowers caused by their different chemical structures. The superhydrophobicity of such functional materials might be beneficial for applications in electrical devices in which the presence of water would influence their performance.

Keywords: hydrophobic effect · materials science · photophysics · self-assembly · superhydrophobic surfaces

Introduction

Diverse nanostructures formed through self-assembly of small aromatic molecules have attracted considerable attention because of their fascinating optical and electronic applications.[1] Noncovalent forces such as hydrogen bonding, π–π stacking, and van der Waals interactions provide the driving force for molecular self-assembly. With the help of new synthetic protocols and characterization techniques, a variety of novel supramolecular architectures have been created. However, full control over the morphologies of self-assembled structures for their implementation in special applications is still a great challenge.

The wettability of a solid surface is an important scientific and practical issue in daily life.[2] Recently, superhydrophobic surfaces inspired by biological microstructures have attracted considerable interest. The morphology of the surface has played a more important role than the chemical composition in determining wettability.[3] In particular, the binary surface structure (micro- and nanostructures) has proven to be optimum for superhydrophobicity.[4] Many approaches, including chemical vapor deposition,[5] laser or plasma etching processes,[6] phase separation,[7] and electrochemical deposition,[8] have been employed to prepare superhydrophobic surfaces. However, self-assembled morphologies using the weak van der Waals interaction have attracted increasing interest in this field.[9,10] Due to the simplicity in their preparation and the diversity of their physical and chemical properties, solution-processable organic materials represent a promising type of material for self-cleaning applications.

Many organic/polymeric materials have been fabricated as superhydrophobic surfaces; however, they usually lack special functionality, since they consist mainly of aliphatic chains. Recently, Nakanishi's group developed a functional superhydrophobic surface by incorporating C_{60} units into a flower-shaped morphology.[9] To introduce more functions into superhydrophobic surfaces, herein we describe the in-

[a] J. Yin, J. Yan, Dr. X. Xu, Prof. K. Wu, Prof. J. Pei
Beijing National Laboratory for Molecular Sciences
The Key Laboratory of Bioorganic Chemistry and Molecular Engineering of the Ministry of Education College of Chemistry and Molecular Engineering Department
Peking University, Beijing 100871 (China)
Fax: (+86) 10-62758145
E-mail: jianpei@pku.edu.cn

[b] M. He, Prof. Y. Song
CAS Key Laboratory of Organic Solids
Institute of Chemistry Chinese Academy of Science
Beijing 100190 (China)
Fax: (+86) 10-62529684
E-mail: ylsong@iccas.ac.cn

Supporting information for this article is available on the WWW under http://dx.doi.org/10.1002/chem.201000332.

corporation of a π-conjugated system into such materials. More specifically, we focused on benzothiophene derivatives, which performed excellently in various devices, such as organic field-effect transistors (OFETs), organic light-emitting diodes (OLEDs), and photovoltaic cells.[11] So far, they have not yet been applied to the formation of hydrophobic surfaces. Therefore, we present new solution-processed flowerlike assemblies formed by these benzodithiophene derivatives, and their applications as superhydrophobic surfaces. The paper is structured as follows: first, we describe the design and synthesis of the molecules used for the self-assembly; second, we detail the morphological studies on our hierarchical micrometer- and nanometer-sized flower-shaped assemblies. By using different characterization techniques, we further investigate the relative role of aliphatic chains and aromatic planes in directing the self-assembly. We also describe in detail the mechanism of how such flowerlike supramolecular structures form. Finally, superhydrophobic surfaces are prepared from the two flowerlike assemblies formed by these benzothiophene derivatives. Our investigation indicates that these flower-shaped morphologies exhibit excellent water-repellent characteristics. In addition, because of the slight microstructure differences in the two kinds of flowers, caused by structural differences between their molecular structures, the transition from the Cassie state with low adhesion to the Wenzel state with high adhesion can be realized. Achieving superhydrophobicity of such functional materials would also be beneficial for their applications in electrical devices in which the presence of water would influence their performance.

Results and Discussion

Design and synthesis of the benzodithiophene derivatives: The "bottom-up" approach suggests that tuning the molecular chemical structures can create new supramolecular structures.[12] To obtain organic three-dimensional self-assemblies, benzodithiophene derivatives with the same aromatic skeleton but different in the substituted positions and number of alkyl chains were synthesized. Compounds **1** and **2** bearing six and two dodecyloxy chains, respectively, were prepared through four steps from the commercially available 1,4-dibromo-2,5-diiodobenzene as shown in Scheme 1. The presence of the conjugated core and long hydrocarbon side chains is expected to facilitate the cooperative interactions of the noncovalent forces between the molecules.

Morphology studies of the self-assemblies: Compounds **1** and **2** were readily soluble in common organic solvents such as THF, $CHCl_3$, and CH_2Cl_2. Compound **1** showed various morphologies after precipitating from different organic solvents as shown in Figure 1. A mixture ($CHCl_3$/EtOH 1:2, v/v) was chosen in the following experiments. Self-assembled morphologies were prepared as follows: first, a suspension of **1** or **2** in the above-mentioned mixture at a concentration of 2 mg mL^{-1} was heated until it formed a transparent solution, and was then allowed to cool slowly to room temperature. Precipitates formed in nearly quantitative yield. For **1**, the images obtained from field-emission scanning electron microscopy (FESEM; Figure 2a and b) and transmission electron microscopy (TEM; Figure 2c and d) revealed an interesting hierarchical structure: an overall

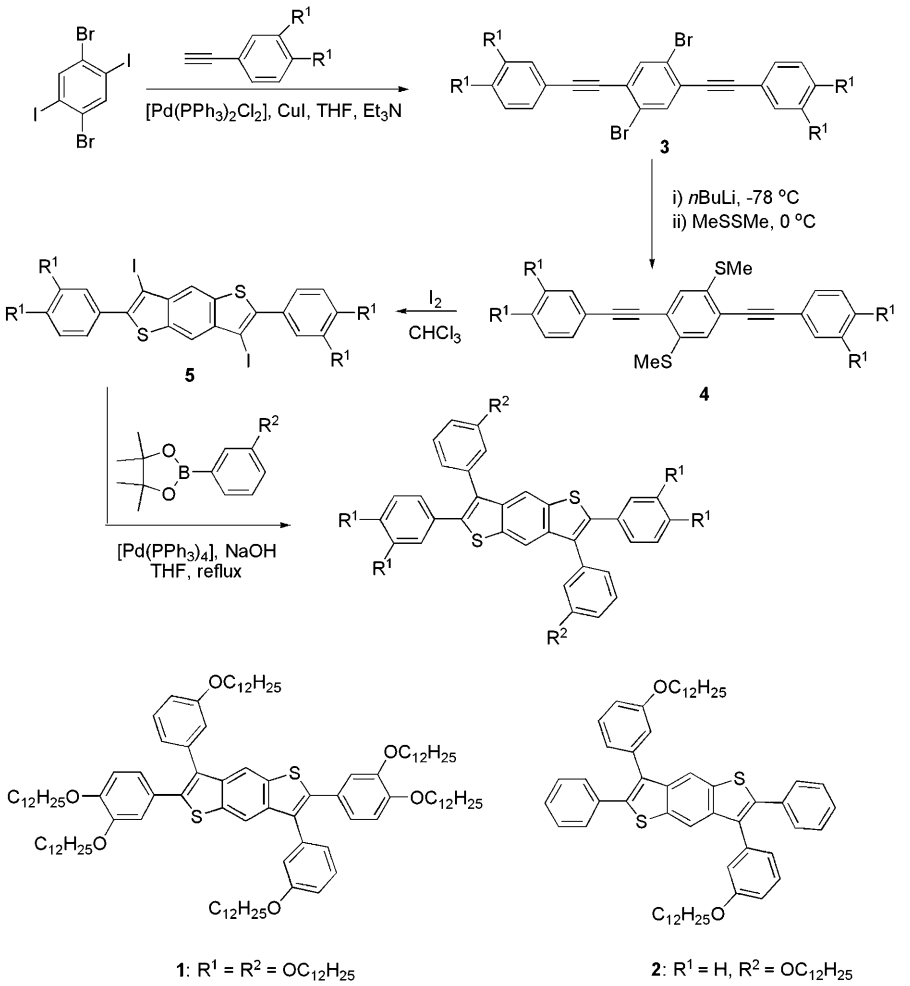

Scheme 1. The synthetic approaches to compounds **1** and **2**.

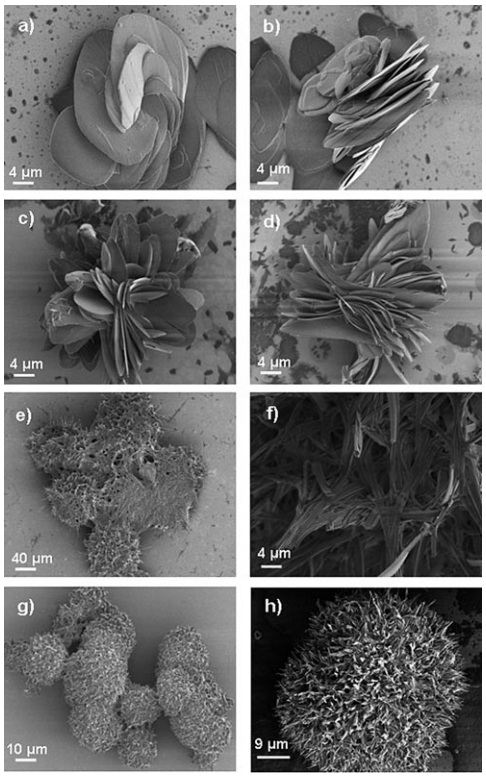

Figure 1. SEM images of **1** precipitated from a), b) *n*-hexane; c), d) 1,4-dioxane; e), f) *n*-dodecane; and g), h) $CHCl_3$/EtOH (1:2 v/v).

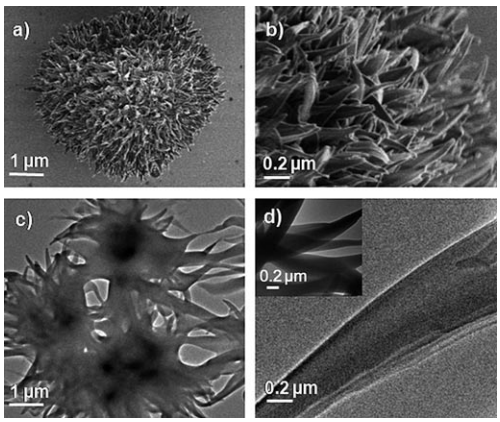

Figure 2. Morphology of self-assembled **1**. a) SEM and c) TEM images of flower-shaped supramolecular assemblies of **1** obtained from $CHCl_3$/EtOH (1:2 v/v). b) SEM and d) TEM images of triangular-like petals of the flower-shaped objects.

flowerlike morphology of several micrometers in size (4–20 μm), built up by numerous triangular-like petals of nanometer size (200–400 nm in length). These petals were acute and arranged closely. In addition, fluorescence microscopy showed that the flower-shaped assemblies exhibited blue fluorescence owing to the π-conjugated aromatic skeleton (Figure S1 in the Supporting Information). For **2**, flower-shaped assemblies with two-tier nanostructures were also observed (Figure 3a and b). In comparison, the size of the

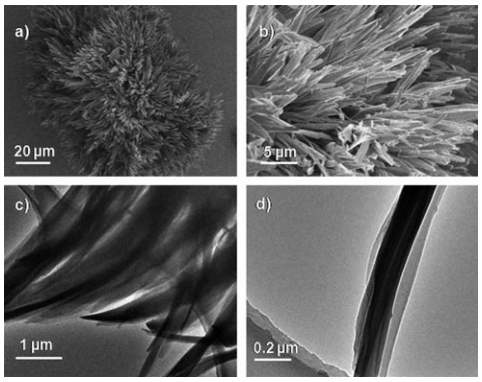

Figure 3. Morphology of self-assembled **2**. a) SEM images of flower-shaped supramolecular assemblies of **2** obtained from $CHCl_3$/EtOH (1:2 v/v). b) SEM and c), d) TEM images of pillarlike petals of the flower-shaped objects.

flowerlike morphology obtained by **2** was much larger than that of **1** (20–50 μm) and consisted of longer pillarlike petals of approximately 5 μm in length and 200 nm in diameter. Figure 3d displays the multilayer structures of the petals, which clearly indicates that the obtained precipitates are formed by hierarchical self-assembly.

Hierarchical organization studies of the flower-shaped structures: The molecular arrangements inside the flower structures were studied by using Fourier transform infrared (FTIR) spectroscopy and powder X-ray diffraction (XRD); their photophysical properties were also investigated. The role of the aliphatic chains in directing crystal-structure formation was reflected in FTIR spectroscopic experiments. FTIR spectra of the flower-shaped supramolecular assemblies **1** and **2** on KBr plates (Figure 4a) showed CH_2 stretching vibrations at 2920 cm^{-1} (ν_{anti}) and 2850 cm^{-1} (ν_{sym}), which indicates crystalline packing of alkyl chains.[13] Powder XRD patterns showed that these flower-shaped objects had a certain degree of crystalline order (Figure 4b). Due to the flower-shaped morphologies, all crystal planes were on average equally exposed, so preferential orientation was not expected. Still, there are strong diffraction signal peaks in the small-angle region corresponding to *d* spacings of 38.7 and 27.0 Å for **1** and **2**, respectively. For **1**, the measured spacing was somewhat smaller than the actual molecular size (47.3 nm horizontally and 44.7 nm vertically), which indicates a certain degree of tilting. Due to the smaller number of alkyl chains, **2** was more anisotropic in shape, so the diffraction pattern was completely different. Typical peaks for aromatic–aromatic stacking (around 3.5 Å) were not observed, because the central parts of the molecules were not planar due to the large torsional angle of aryl groups on the vertical axis;[14] this can be established by viewing the molecular structures calculated by utilizing the Gaussian 03 program (see the Supporting Information).[15,16]

On the other hand, the importance of the central aromatic unit in the self-assembly is revealed from the change in the

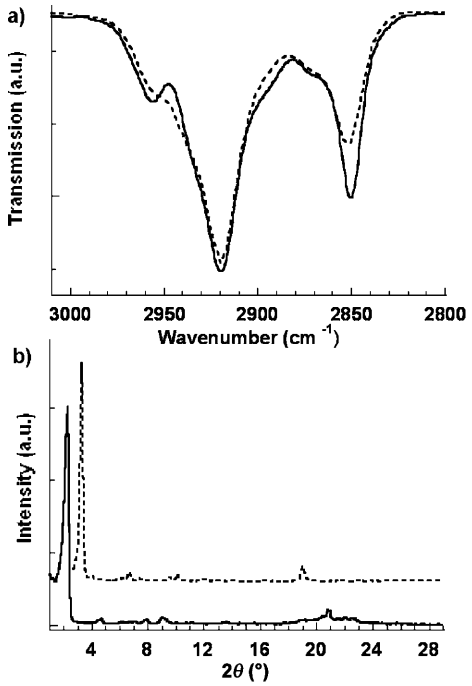

Figure 4. a) FTIR spectra (KBr) and b) powder X-ray diffraction data of **1** (——) and **2** (-----) precipitated from $CHCl_3$/EtOH (1:2 v/v).

absorption and emission spectra on going to the solid state. In various dilute organic solutions, **1** showed almost identical absorption features with two major bands at about 290 and 360 nm as shown in Figure S2 in the Supporting Information. The UV-visible features of a drop-cast film of the flower-shaped structures of **1** showed an absorption maximum at 400 nm, which redshifted 30 nm relative to that in its dilute solution (1×10^{-5} M) in chloroform, as shown in Figure 5a. Such a large redshift indicates strong interactions among conjugated plains in the solid state, which changed its photophysical properties.[17,18] Upon heating the mixture of **1** in $CHCl_3$/EtOH (1:2 v/v) to 60 °C, the redshifted band of the absorption maximum disappeared and the original band at 360 nm recurred. Such behavior was also demonstrated by its emission features in Figure 5b, in which the emission maximum (λ_{max}) also showed a considerable redshift on going from the solution to the solid state. Similar to **1**, the absorption and emission spectra of **2** under the abovementioned conditions also experience similar changes (Figure 5c and d). These observations revealed that in chloroform and in the $CHCl_3$/EtOH (1:2 v/v) mixture at 60 °C, **1** and **2** were in their monomeric form. However, as the solution temperature decreased from 60 °C to room temperature, the formation of self-assembled species occurred.[19]

In general, based on these results obtained from FTIR spectroscopy, XRD, optical properties, and micrograph analyses, we tentatively conclude that the self-assembly of **1** and **2** was assisted by the electronic interaction of the aromatic skeleton and the weak van der Waals interactions of long aliphatic chains. The exact crystal structure of these precipitates remains unknown at this stage.

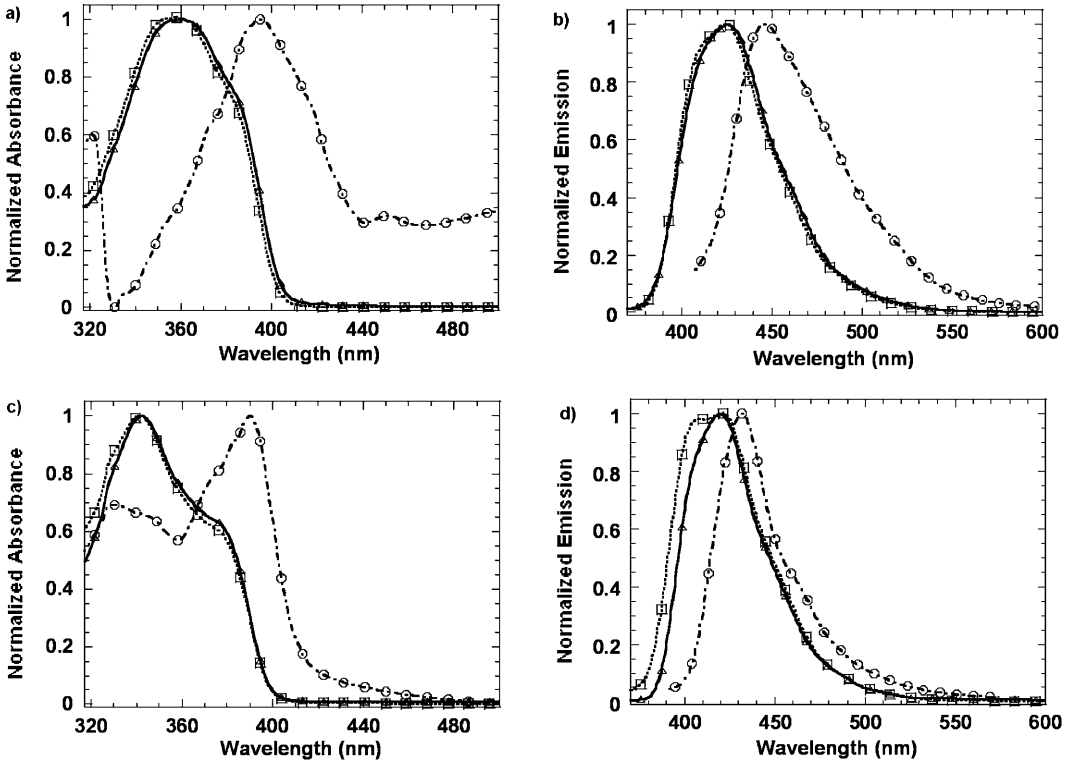

Figure 5. a) Normalized absorption and b) emission spectra of **1**; and c) normalized absorption and d) emission spectra of **2** in $CHCl_3$ (△) ([**1**] = 1×10^{-5} M), $CHCl_3$/EtOH (1:2 v/v) at 60 °C (□) ([**1**] = 1×10^{-5} M), and drop-cast films (○) of the suspension of flower-shaped structures.

The formation mechanism of flower-shaped supramolecular assemblies: It is interesting to trace the formation mechanism of the flower-shaped objects. First, we slowly cooled down a homogeneous mixture of the compounds in $CHCl_3$/EtOH (1:2 v/v) from 60°C to room temperature, which yielded intermediate assembled structures of the precipitates. Then, one drop of the suspension of the assembled objects was deposited on Si, and excess solvent on the silicon plate was quickly drained off with filter paper.

As shown in Figure 6, only platelike and elliptical precursors were observed at the initial stage for **1**. We note that such flat objects consisted of stacked layers instead of a single layer (also observed in ref. [9a]), as supported by control experiments mentioned later. The edges of such precursors started to bifurcate in every direction (Figure 6a, b, and c), and then to roll up to minimize the total elastic energy.[20] When the rolling-up behavior proceeded continuously, the inner layers had more space to consequently bifurcate (Figure 6d and e), resulting in a 3D flower-shaped object. After enough bifurcation growth at the edges and folding in the plate, the transformation was complete. Rapid cooling from 60 to 0°C produced only platelike, elliptical assemblies (Figure 6g, h, and i). Obviously, because of the rapid cooling process, those precursors had no time for the bifurcation and rolling-up, resulting in exclusive formation of intermediate assembled structures, which are very rare in surfactant assemblies. In addition to individual flower-shaped objects, we also observed "clustered flowers" (Figure 6j, k, and l) in our samples. It was unlikely that these flowers experienced only physical entanglement, judging from the SEM pictures. We suspected that some large plates (precursors) were connected together at the initial stage and later evolved into such large clusters.

Similarly, rapid cooling of the homogeneous mixture of **2** in $CHCl_3$/EtOH (1:2 v/v) to 0°C produced multilayered, micrometer-sized belts, which indirectly proved that the sheet precursors (Figure 7a) obtained by slow cooling to 50°C were also multilayered. As the slow aging proceeds continuously, the objects start to bifurcate all around (Figure 7b), which results in the assemblies with scrolled petals (Figure 7c and d). Then every scrolled petal was stretched until the whole system was energetically stable (Figure 7e and f), leading to the final structures of the flower-shaped three-dimensional objects.

The formation mechanism described above indicates that the formation of the microscopic flower-like assemblies was determined by both the spatial and energy factors during the growth process. In addition, slow aging was essential for the formation of flower-shaped assemblies.

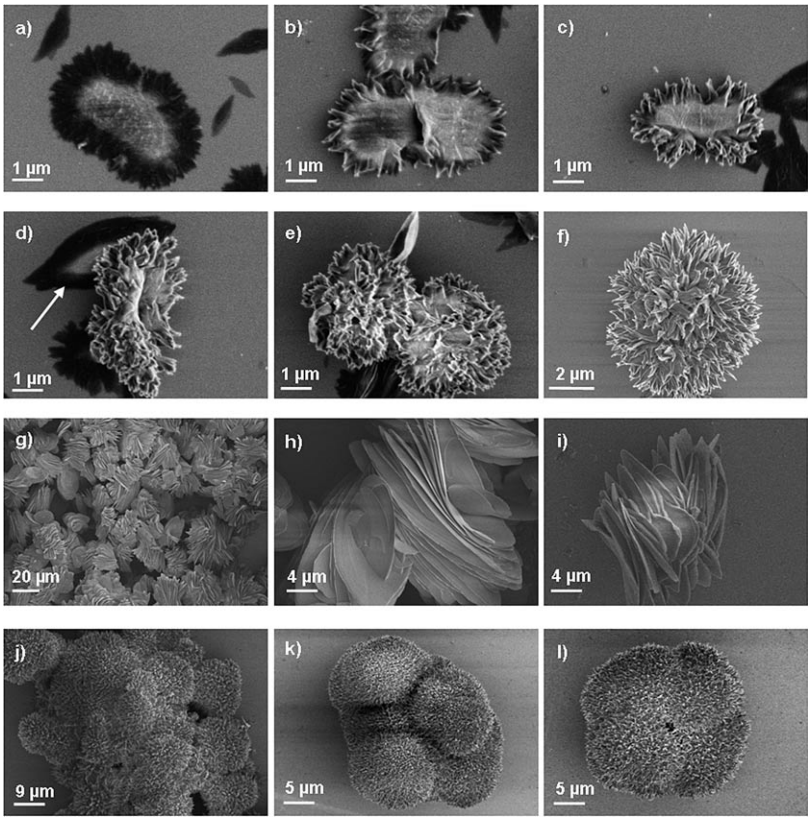

Figure 6. SEM images of intermediates of flower-shaped supramolecular assemblies of **1** when slowly cooling a hot homogeneous solution of **1** in $CHCl_3$/EtOH from 60°C to a) 50°C ; b) 45°C ; c) 40°C ; d) 35°C (the arrow shows the possible precursor for the flower formation); e) 30°C ; f) 25°C. g)–i) SEM images of multilayer assemblies of **1** formed by rapid cooling from 60 to 0°C. j)–l) SEM images of "clustered flowers".

The properties of superhydrophobic surfaces: The surface of a lotus leaf consists of papillose epidermal cells on a micrometer scale with a branchlike nanostructure on every papilla.[4b,21] Such a dual-scale roughness gives the surface excellent superhydrophobicity: water droplets can roll off the surfaces with dirt and contamination without wetting the surfaces. Because of the resemblance of our hierarchical structures to that of the lotus leaf, we tried to obtained superhydrophobic surfaces using our new flower-shaped objects.

Both of the morphologies we obtained can be easily fabricated on various substrates (e.g., silicon, metal, and glass) by drop-casting. Under these conditions, flower-shaped objects formed densely packed films (Figure 8b). Figure 8a is an image of a water droplet (6 μL) lying on a thin film of **1**. The static contact angle (CA) of water on the thin film was measured to be 156.5° (Figure 8c). The water droplet could roll on

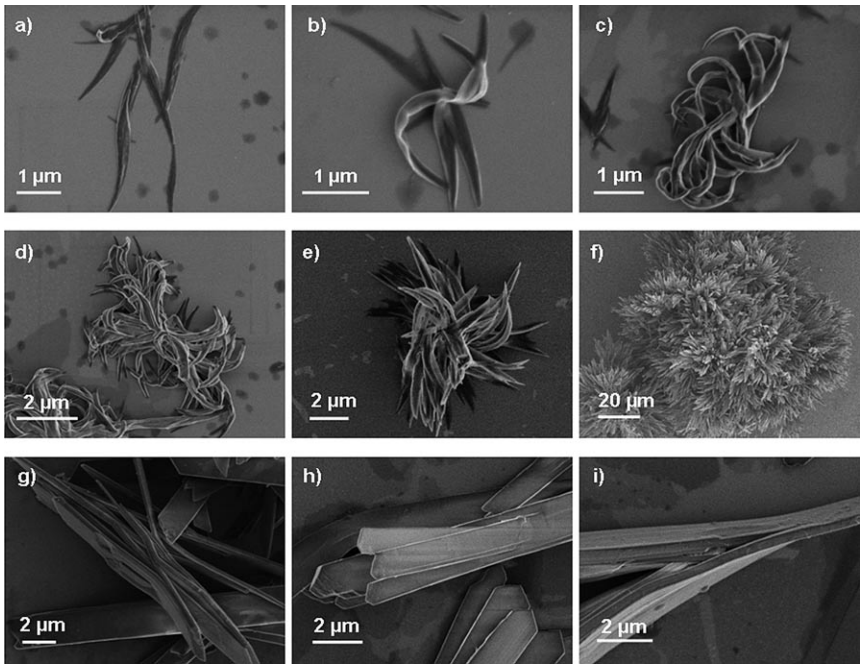

Figure 7. SEM images of intermediates of flower-shaped supramolecular assemblies of **2** when slowly cooling a hot homogeneous solution of **2** in $CHCl_3$/EtOH from 60 °C to a), b) 50 °C; c), d) 40 °C; e) 35 °C ; f) 25 °C. g)–i) SEM images of multilayer assemblies of **2** formed by rapid cooling from 60 to 0 °C.

the thin film freely when being pulled with a needlepoint. In contrast, a spin-coated film of **1** from a solution in chloroform onto silicon resulted in a smooth layer with a low surface roughness (2 nm as measured by atomic force microscopy (AFM); Figure 8d), and exhibited a static contact angle of only 102.7° (inset of Figure 8d), even though they were formed by the same chemical structure. In the same way, self-assembled **2** also had a binary surface structure (micro- and nanostructures), and the surface of **2** showed the superhydrophobicity with a water CA of 155.8° (Figure 9d), in contrast to the CA of 103.1° (Figure 9c) on the spin-coated film from the solution of **2** in $CHCl_3$. This striking contrast demonstrated the importance of the rough, two-tier surface structures on the wettability of the solid structure.

Contact-angle hysteresis, which is determined by the air–liquid–solid three-phase contact line, can be used to infer the sliding behavior of a water droplet on a surface. Generally, there are two superhydrophobic states on a rough surface: Wenzel's state and Cassie's state.[22,23] Water droplets in Wenzel wetting are found to be highly adhesive (the high CA hysteresis); on the other hand, those in a Cassie wetting state can roll off easily (low CA hysteresis). Figure 8e shows that the sliding angle (SA) in the thin film formed from flower-shaped objects **1** was smaller than 3°. The small sliding angle indicated that the water droplet was suspended by the air trapped on the composite contact surface[24] and could easily roll down the surface when tilted, just like the lotus surface in a Cassie's state. In contrast to the morphologies of **1**, the size of hierarchical micro- and nanostructures of **2** were both larger than those of **1**. Accordingly, the surface morphology prepared for a large amount of flower objects of **2** looked different to that of **1** (Figure 8b). There were many microscale pillar-shaped microstructures on the superhydrophobic surfaces of **2** (Figure 9a and b). This demonstrated that water could easily penetrate into the grooves on the surface of **2**, because of the strong capillary force of the pillar-shaped microstructures, resulting in the superhydrophobicity with high adhesive force (Wenzel's state; Figure 10).[25] The result was exactly what we expected: water droplets stayed pinned to the surface of **2** when the surface was tilted (Figure 9e) or even when it was turned upside down (Figure 9f).

In addition, a series of pictures, following the time sequence, of a water droplet striking our superhydrophobic surfaces showed the differences of the two surfaces more vividly (Figure 11). The shape of the water droplet changes dramatically during striking as its kinetic energy transforms into potential energy due to the deformation of its shape.[26] Despite these deformations, the droplets falling from the same height toward the two different surfaces could return to their round shape and both bounced back in 16 ms because the surfaces were very water repellent. However, during the second stroke in succession, because of the high adhesion force, the water droplet on the surface of the flower-shaped **2** became almost static (Figure 11b), whereas it could rebound several times on the surface of **1** (Figure 11a). The facts also indicate the difference of surface adhesion caused by the two dual-scale microstructures.

The static contact angle and sliding angle of the obtained films of globular objects did not change with time for at least two weeks at room temperature, thus showing some degree of stability. The fractal morphologies of the prepared superhydrophobic films could be stabilized below their melting points (104.1 and 187.3 °C for **1** and **2**, respectively; Figure S3 in the Supporting Information).[27] In addition, it is noteworthy that compared with other methods used for the preparation of superhydrophobic surfaces, our films were readily prepared by means of an easy solution process, and could be readily re-formed, re-used, or washed away.

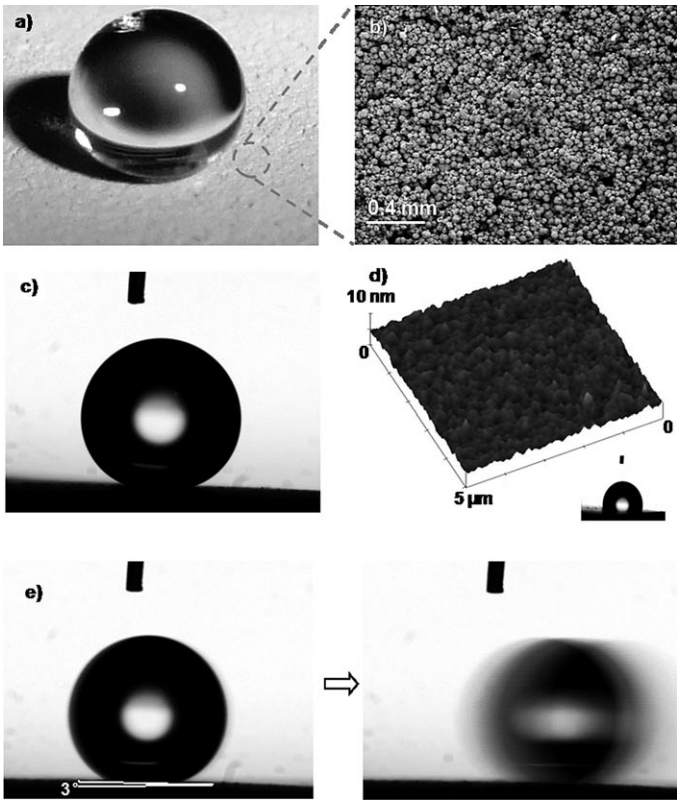

Figure 8. a) Picture of a water droplet on a film of **1**. b) SEM image of a film of **1** on Si deposited from $CHCl_3$/EtOH (1:2 v/v). c) Photograph of a water droplet on the surface (contact angle of 156.5°). d) AFM image of **1** on Si spin-coated film from the solution of **1** in $CHCl_3$ (the roughness in height was about 2 nm), and a photograph (inset) of a water droplet on the spin-coated film (contact angle of 102.7°). e) Images obtained during sliding angle measurement, which indicate that a water droplet can roll down the thin film of the globular object's surface easily.

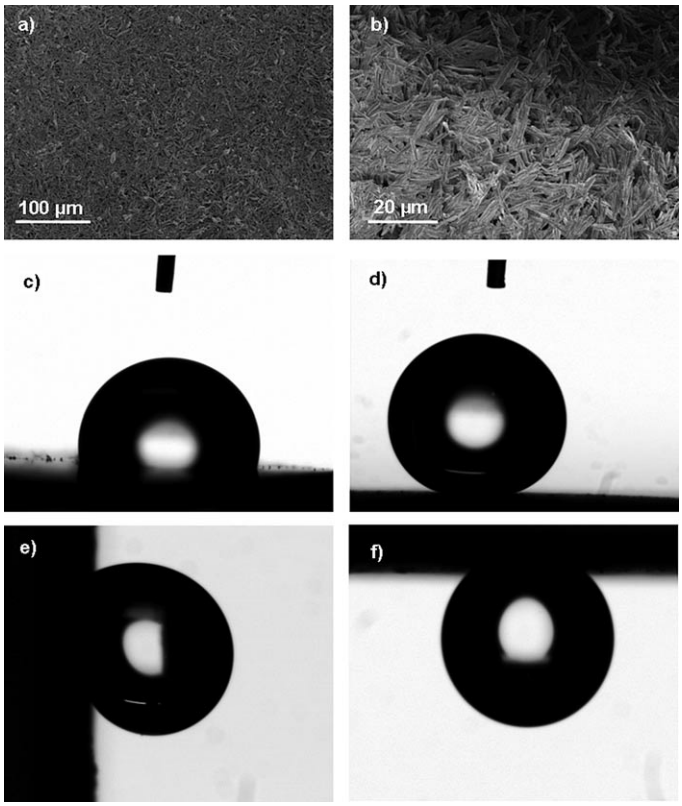

Figure 9. a), b) SEM images of a film of **2** on Si deposited from $CHCl_3$/EtOH (1:2 v/v). c) Behavior of water droplet on a spin-coated film from a solution of **2** in $CHCl_3$ (CA of 103.1°). Shapes of water droplets on a film of **2** on Si deposited from its solution in $CHCl_3$/EtOH (1:2 v/v) with different tilt angles: d) 0°, CA of 155.8 °C, e) 90°, f) 180°.

Conclusion

In summary, by means of a slight adjustment of alkyl chains of the molecular structure, two kinds of microscale flower-shaped morphologies with nanometer petals have been formed through hierarchical self-assemblies of benzodithiophene derivatives. By capturing intermediate stages of the assemblies, we have proposed a new formation mechanism for such a flower-shaped morphology. The hierarchical morphologies of the films allowed us to fabricate superhydrophobic surfaces by means of a simple solution process. Two different surfaces with a Cassie state and Wenzel state have been realized. The water-repelling characteristics of surfaces formed by **1** are comparable to that of the lotus leaf (contact angle larger than 161.0° and sliding angle of about 2°), and another surface has a high adhesive property as the flower's petals. The superhydrophobicity of the surfaces was vividly visualized through the investigation of the free-falling water droplets striking the films. The comparison of these results with that of a flat film formed with the same molecular structure but without the dual-scale roughness, demonstrates the importance of the hierarchical structure. We are now exploring other applications of the as-prepared films, such as chemical sensors[28] and supramolecular templates,[29] with an aim to develop new functional devices that can work in ambient conditions or even in water.

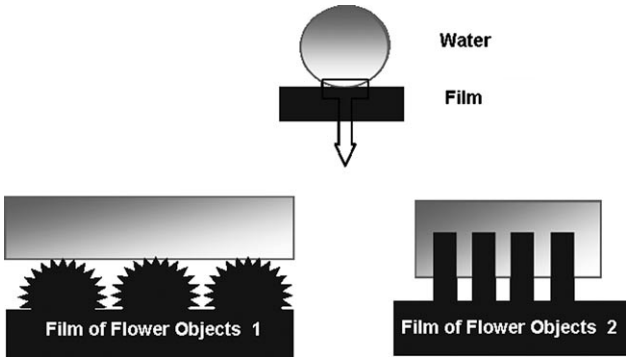

Figure 10. A schematic illustration for describing the local interaction of a drop of water in contact with the film of flower objects.

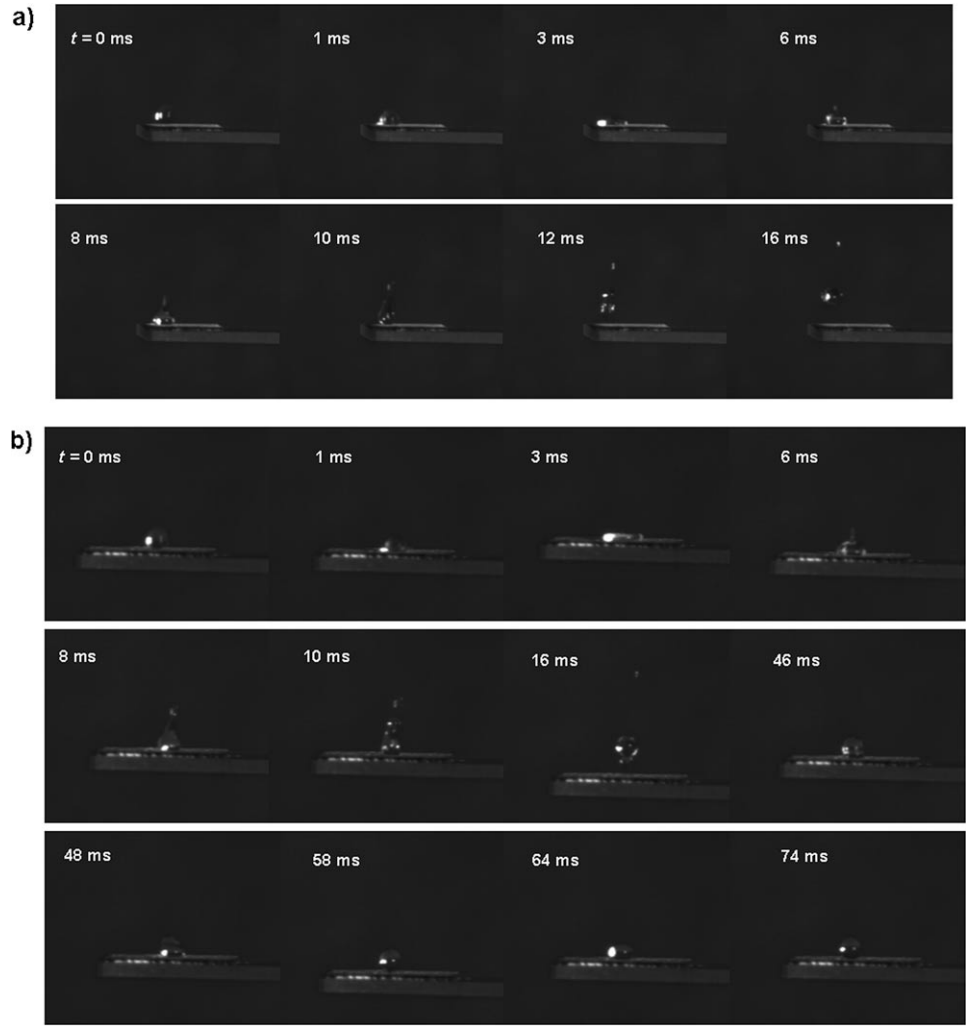

Figure 11. Selected snapshots of a water droplet striking our superhydrophobic surfaces of a) **1** and b) **2**.

Experimental Section

Reagents and instrumentation: All commercially available chemicals were used without further purification unless otherwise noted. CH_2Cl_2 was distilled from CaH_2 under nitrogen. THF was freshly distilled from sodium and benzophenone ketyl under nitrogen prior to use. Column chromatography was performed with silica gel (0.063–0.2 mm). All yields given refer to isolated yields. ^1H and ^{13}C NMR spectra were recorded on Mercury plus 300 MHz and Bruker 400 MHz instruments using $CDCl_3$ as solvent unless otherwise noted. ^1H NMR chemical shifts were referenced to TMS ($\delta = 0$ ppm) or $CHCl_3$ ($\delta = 7.26$ ppm), and ^{13}C NMR chemical shifts were referenced to $CDCl_3$ ($\delta = 77.00$ ppm). High-resolution (HR) ESI mass spectra were recorded on a Bruker Apex IV FTMS. Differential scanning calorimetry (DSC) analyses were performed on a Mettler Toledo Instrument DSC822e calorimeter. Powder X-ray diffraction analyses were recorded on a D/max-RA high-power rotating anode 12 kW X-ray diffractometer. All AFM experiments were carried out with a Nanoscope IIIa microscope (Multimode, Digital Instruments) under ambient conditions. Absorption spectra were recorded on a Perkin–Elmer Lambda 35 UV-visible spectrometer. Photoluminescence (PL) spectra were carried out on a Perkin–Elmer LS55 luminescence spectrometer. Scanning electron microscopy (SEM) was performed on a Philips XL30W/TMP operating at 1 kV. Transmission electron microscopy (TEM) was recorded on a Philips model Tecnai F20 electron microscope operating at 120 kV.

Water-repellent and adhesive properties: The sessile drop method was used for CA measurements with a dataphysics OCA20 contact angle system at 22 °C. The water droplet size used for measurements was 3.0 μL. The contact angles were measured at five different points of each sample.

Compound 3: A mixture of THF (50 mL) and triethylamine (15 mL) was added to a mixture of 1,4-dibromo-2,5-diiodobenzene (1.00 g, 2.05 mmol), 1,2-bis(dodecyloxy)-4-ethynylbenzene (1.97 g, 4.2 mmol), $[PdCl_2(PPh_3)_2]$ (115 mg, 0.12 mmol), and CuI (11 mg, 0.06 mmol) under nitrogen using syringes. After it had been stirred overnight at room temperature under nitrogen, the mixture was poured into saturated aqueous NH_4Cl solution (100 mL). Aqueous layers were extracted with EtOAc. The combined organic layers were washed with brine, and then dried over Na_2SO_4. After removal of the solvents under reduced pressure, the residue was purified by column chromatography (silica gel, petroleum ether/chloroform 5:1) to give **3** as a white solid. Yield: 1.92 g, 80%; ^1H NMR (300 MHz, $CDCl_3$): $\delta = 7.74$ (s, 2H), 7.16–7.12 (dd, $J = 8.4$, 1.8 Hz, 2H), 7.05–7.04 (d, $J = 1.8$ Hz, 2H), 6.85–6.83 (d, $J = 8.4$ Hz, 2H), 4.03–3.99 (m, 8H), 1.85–1.78 (m, 8H), 1.47–1.27 (m, 72H), 0.95–0.86 ppm (t, $J = 6.9$ Hz, 12H); ^{13}C NMR (75 MHz, $CDCl_3$): $\delta =$ 150.5, 148.8, 135.7, 126.3, 125.4, 123.4, 116.8, 114.4, 113.2, 97.2, 85.6, 69.3, 69.1, 31.9, 29.69, 29.66, 29.63, 29.41, 29.36, 29.23, 29.18, 26.0, 22.7, 14.1 ppm; HRMS (ESI): m/z calcd for $C_{70}H_{109}Br_2O_4$: 1171.6692 $[M+1]^+$; found: 1171.6706.

Compound 4: nBuLi (2.5 M in hexane, 0.6 mL) was added dropwise to a solution of compound **3** (500 mg, 0.43 mmol) in anhydrous Et_2O (100 mL) under nitrogen at −78 °C. After 10 min at −78 °C, the mixture was stirred at 0 °C for 1 h, and then dimethyl disulfide (160 mg, 1.7 mmol) was added using a syringe. The mixture was stirred at room temperature for 4 h, and then poured into an aqueous NH_4Cl solution. The organic layer was washed with saturated NH_4Cl, brine, and then dried over Na_2SO_4. After removal of the solvents under reduced pressure, the residue was purified by column chromatography (silica gel, petroleum ether/dichloromethane 8:1) to give **4** as a yellow solid. Yield: 350 mg, 73%; ^1H NMR (300 MHz, $CDCl_3$): $\delta = 7.16$–7.14 (dd, $J = 8.4$, 1.8 Hz, 2H), 7.074–7.069 (d, $J = 1.8$ Hz, 2H), 6.85–6.83 (d, $J = 8.4$ Hz, 2H), 4.03–3.95 (m, 8H), 2.52 (s, 6H) 1.86–1.79 (m, 8H), 1.49–1.26 (m, 72H), 0.90–0.86 ppm (t, $J = 6.9$ Hz, 12H); ^{13}C NMR (100 MHz, $CDCl_3$): $\delta = 150.1$, 148.8, 137.3, 127.7, 125.2, 122.1, 116.7, 114.9, 113.2, 113.1, 97.8, 85.3, 69.3, 69.2, 69.1, 31.9, 29.7, 29.65, 29.62, 29.61, 29.4, 29.35, 29.3, 29.2, 29.18, 29.1, 26.0, 25.99, 22.7, 15.4, 14.1 ppm; HRMS (ESI): m/z calcd for $C_{72}H_{115}O_4S_2$: 1107.8231 $[M+1]^+$; found: 1107.8230.

Compound 5: Iodine (367 mg, 1.44 mmol) was added to a solution of compound **4** (400 mg, 0.36 mmol) in $CHCl_3$ (100 mL). After 1 h, aqueous sodium thiosulfate (2 M, 10 mL) was added. The organic layer was washed with brine, and then dried over Na_2SO_4. After removal of the solvents under reduced pressure, the residue was recrystallized in $CHCl_3/CH_2Cl_2$

to give **5** as a yellow solid. Yield: 433 mg, 90%; ^{1}H NMR (300 MHz, $CDCl_3$): δ = 8.21 (s, 2H), 7.32–7.31 (d, J = 2.1 Hz, 2H), 7.27–7.23 (dd, J = 1.8, 8.4 Hz, 2H), 6.97–6.95 (d, J = 8.4 Hz, 2H), 4.12–4.04 (m, 8H), 1.89–1.84 (m, 8H), 1.50–1.26 (m, 72H), 0.90–0.85 ppm (m, J = 6.9 Hz, 12H); ^{13}C NMR (75 MHz, $CDCl_3$): δ = 150.1, 148.8, 143.5, 140.7, 136.7, 126.9, 122.9, 119.1, 115.6, 115.5, 113.2, 69.6, 69.56, 69.47, 69.2, 31.9, 29.7, 29.6, 29.5, 29.44, 29.36, 29.28, 26.1, 22.7, 14.1 ppm; HRMS (ESI): m/z calcd for $C_{70}H_{108}I_2O_4S_2$: 1330.5772 $[M+1]^+$; found: 1330.5778.

Compound 1: Deionized water (1 mL) was added to a mixture of **5** (200 mg, 0.15 mmol), NaOH (60 mg, 1.5 mmol), 3-dodecyloxyphenylboronic acid pinacol ester (120 mg, 0.31 mmol), and $[Pd(PPh_3)_4]$ (14 mg, 0.01 mmol) in THF (40 mL) under nitrogen by using syringes. After it had been left at reflux at 80 °C for 10 h, the mixture was poured into water (100 mL). The aqueous layer was extracted with EtOAc. The combined extracts were washed with saturated NH_4Cl, brine, and then dried over Na_2SO_4. After removal of the solvents under reduced pressure, the residue was purified by column chromatography over silica gel (petroleum ether/$CHCl_3$ 7:1) to give **1** as a yellow solid. Yield: 205 mg, 85%; ^{1}H NMR (400 MHz, $CDCl_3$): δ = 7.95 (s, 2H), 7.38–7.34 (m, 2H), 7.00–6.93 (m, 8H), 6.79 (s, 2H), 6.77 (s, 2H), 3.98–3.95 (t, J = 6.6 Hz, 4H), 3.93–3.89 (t, J = 6.6 Hz, 4H), 3.64–3.61 (t, J = 6.6 Hz, 4H), 1.83–1.61 (m, 12H), 1.44–1.26 (m, 108H), 0.90–0.86 ppm (m, 18H); ^{13}C NMR (75 MHz, $CDCl_3$): δ = 159.6, 148.8, 148.4, 139.9, 139.3, 137.5, 135.8, 131.1, 129.9, 126.8, 122.7, 121.8, 116.3, 115.8, 114.5, 113.9, 113.1, 69.1, 68.7, 68.1, 31.9, 29.74, 29.68, 29.65, 29.62, 29.43, 29.36, 29.2, 29.0, 26.1, 25.99, 25.92, 22.7, 14.1 ppm; HRMS (ESI): m/z calcd for $C_{106}H_{166}O_6S_2$: 1599.2120 $[M+1]^+$; found: 1599.2131.

Compound 2: The preparation of compound **2** was carried out on a scale of 0.15 mmol using the same procedure as for the preparation of compound **1**. Yield: 104 mg, 80%; ^{1}H NMR (400 MHz, $CDCl_3$): δ = 8.05 (s, 2H), 7.37–7.33 (m, 6H), 7.27–7.23 (m, 6H), 6.97–6.92 (m, 6H), 3.92–3.88 (t, J = 6.6 Hz, 4H), 1.77–1.70 (m, 4H), 1.41–1.26 (m, 36H), 0.89–0.85 ppm (m, 6H); ^{13}C NMR (75 MHz, $CDCl_3$): δ = 159.4, 140.0, 139.2, 136.9, 136.2, 134.3, 132.1, 129.8, 129.5, 128.3, 127.8, 122.7, 116.3, 116.25, 114.2, 68.1, 31.9, 29.7, 29.63, 29.60, 29.57, 29.4, 29.3, 29.2, 26.0, 22.7, 14.1 ppm; HRMS (ESI): m/z calcd for $C_{58}H_{70}O_2S_2$: 862.4812 $[M]^+$; found: 862.4829.

Acknowledgements

This work was supported by the Major State Basic Research Development Program (nos. 2006CB921602 and 2009CB623601) from the Ministry of Science and Technology, and National Natural Science Foundation of China. We thank Professor Yizhuang Xu for fluorescence microscopy measurements.

[1] a) A. Ajayaghosh, S. J. George, *J. Am. Chem. Soc.* **2001**, *123*, 5148; b) P. Jonkheijm, A. Miura, M. Zdanowska, F. J. M. Hoeben, S. De Feyter, A. P. H. J. Schenning, F. C. De Schryver, E. W. Meijer, *Angew. Chem.* **2004**, *116*, 76; *Angew. Chem. Int. Ed.* **2004**, *43*, 74; c) L. Zang, Y. Che, J. S. Moore, *Acc. Chem. Res.* **2008**, *41*, 1596; d) L. C. Palmer, S. I. Stupp, *Acc. Chem. Res.* **2008**, *41*, 1674; e) W. Jin, Y. Yamamoto, T. Fukushima, N. Ishii, J. Kim, K. Kato, M. Takata, T. Aida, *J. Am. Chem. Soc.* **2008**, *130*, 9434.

[2] a) L. Qu, L. Dai, M. Stone, Z. Xia, Z. L. Wang, *Science* **2008**, *322*, 238; b) X. Wu, G. Shi, *J. Phys. Chem. B* **2006**, *110*, 11247.

[3] a) T. Sun, L. Feng, X. Gao, L. Jiang, *Acc. Chem. Res.* **2005**, *38*, 644; b) X.-M. Li, D. Reinhoudt, M. Crego-Calama, *Chem. Soc. Rev.* **2007**, *36*, 1350; c) F. Xia, L. Jiang, *Adv. Mater.* **2008**, *20*, 2842; d) X. Zhang, F. Shi, J. Niu, Y. Jiang, Z. Wang, *J. Mater. Chem.* **2008**, *18*, 621.

[4] a) D. Öner, T. J. McCarthy, *Langmuir* **2000**, *16*, 7777; b) L. Feng, S. Li, Y. Li, H. Li, L. Zhan, J. Zhai, Y. Song, B. Liu, L. Jiang, D. Zhu, *Adv. Mater.* **2002**, *14*, 1857; c) K. K. S. Lau, J. Bico, K. B. K. Teo, M. Chhowalla, G. A. J. Amaratunga, W. I. Milne, G. H. McKinley, K. K. Gleason, *Nano Lett.* **2003**, *3*, 1701; d) I. A. Larmour, S. E. J. Bell, G. C. Saunders, *Angew. Chem.* **2007**, *119*, 1740; *Angew. Chem. Int. Ed.* **2007**, *46*, 1710; e) Y. Kwon, N. Patankar, J. Choi, J. Lee, *Langmuir* **2009**, *25*, 6129.

[5] L. Huang, S. P. Lau, H. Y. Yang, E. S. P. Leong, S. F. Yu, *J. Phys. Chem. B* **2005**, *109*, 7746.

[6] K. Teshima, H. Sugimura, Y. Inoue, O. Takai, A. Takano, *Appl. Surf. Sci.* **2005**, *244*, 619.

[7] a) H. Y. Erbil, A. L. Demirel, Y. Avci, O. Mert, *Science* **2003**, *299*, 1377; b) Q. Xie, G. Fan, N. Zhao, X. Guo, J. Xu, J. Dong, L. Zhang, Y. Zhang, C. C. Han, *Adv. Mater.* **2004**, *16*, 1830.

[8] N. J. Shirtcliffe, G. McHale, M. I. Newton, C. C. Perry, *Langmuir* **2005**, *21*, 937.

[9] a) T. Nakanishi, K. Ariga, T. Michinobu, K. Yoshida, H. Takahashi, T. Teranishi, H. Möhwald, D. G. Kurth, *Small* **2007**, *3*, 2019; b) T. Nakanishi, T. Michinobu, K. Yoshida, N. Shirahata, K. Ariga, H. Möhwald, D. G. Kurth, *Adv. Mater.* **2008**, *20*, 443.

[10] S. Srinivasan, V. K. Praveen, R. Philip, A. Ajayaghosh, *Angew. Chem.* **2008**, *120*, 5834; *Angew. Chem. Int. Ed.* **2008**, *47*, 5750.

[11] a) Y. Zhou, W. Liu, Y. Ma, H. Wang, L. Qi, Y. Cao, J. Wang, J. Pei, *J. Am. Chem. Soc.* **2007**, *129*, 12386; b) Q. Niu, Y. Zhou, L. Wang, J. Peng, J. Wang, J. Pei, Y. Cao, *Adv. Mater.* **2008**, *20*, 964; c) L. Wang, Y. Zhou, J. Yan, J. Wang, J. Pei, Y. Cao, *Langmuir* **2009**, *25*, 1306; d) J. E. Anthony, *Chem. Rev.* **2006**, *106*, 5028; e) J. L. Brusso, O. D. Hirst, A. Dadvand, S. Ganesan, F. Cicoira, C. M. Robertson, R. T. Oakley, F. Rosei, D. F. Perepichka, *Chem. Mater.* **2008**, *20*, 2484; f) A. Mishra, C.-Q. Ma, P. Bäuerle, *Chem. Rev.* **2009**, *109*, 1141.

[12] M. G. Ryadnov, D. N. Woolfson, *J. Am. Chem. Soc.* **2005**, *127*, 12407.

[13] a) J. P. Hill, W. Jin, A. Kosaka, T. Fukushima, H. Ichihara, T. Shimomura, K. Ito, T. Hashizume, N. Ishii, T. Aida, *Science* **2004**, *304*, 1481; b) G. John, M. Masuda, Y. Okada, K. Yase, T . Shimizu, *Adv. Mater.* **2001**, *13*, 715.

[14] R. Shukla, S. H. Wadumethrige, S. V. Lindeman, R. Rathore, *Org. Lett.* **2008**, *10*, 3587.

[15] Gaussian 03, Revision C.02, M. J. Frisch, G. W. Trucks, H. B. Schlegel, G. E. Scuseria, M. A. Robb, J. R. Cheeseman, J. A. Montgomery, Jr., T. Vreven, K. N. Kudin, J. C. Burant, J. M. Millam, S. S. Iyengar, J. Tomasi, V. Barone, B. Mennucci, M. Cossi, G. Scalmani, N. Rega, G. A. Petersson, H. Nakatsuji, M. Hada, M. Ehara, K. Toyota, R. Fukuda, J. Hasegawa, M. Ishida, T. Nakajima, Y. Honda, O. Kitao, H. Nakai, M. Klene, X. Li, J. E. Knox, H. P. Hratchian, J. B. Cross, C. Adamo, J. Jaramillo, R. Gomperts, R. E. Stratmann, O. Yazyev, A. J. Austin, R. Cammi, C. Pomelli, J. W. Ochterski, P. Y. Ayala, K. Morokuma, G. A. Voth, P. Salvador, J. J. Dannenberg, V. G. Zakrzewski, S. Dapprich, A. D. Daniels, M. C. Strain, O. Farkas, D. K. Malick, A. D. Rabuck, K. Raghavachari, J. B. Foresman, J. V. Ortiz, Q. Cui, A. G. Baboul, S. Clifford, J. Cioslowski, B. B. Stefanov, G. Liu, A. Liashenko, P. Piskorz, I. Komaromi, R. L. Martin, D. J. Fox, T. Keith, A. Laham, C. Y. Peng, A. Nanayakkara, M. Challacombe, P. M. W. Gill, B. Johnson, W. Chen, M. W. Wong, C. Gonzalez, J. A. Pople, Gaussian Inc., Wallingford CT, **2004**.

[16] GaussView, Version 3.09, R. Dennington II, T. Keith, J. Millam, K. Eppinnett, W. L. Hovell, R. Gilliland, Semichem, Inc., Shawnee Mission KS, **2003**.

[17] J.-Y. Wang, J. Yan, Z. D. Li, J.-M. Han, Y. Ma, J. Bian, J. Pei, *Chem. Eur. J.* **2008**, *14*, 7760.

[18] S. Yagai, T. Seki, T. Karatsu, A. Kitamura, F. Würthner, *Angew. Chem.* **2008**, *120*, 3415; *Angew. Chem. Int. Ed.* **2008**, *47*, 3367.

[19] S. J. George, A. Ajayaghosh, *Chem. Eur. J.* **2005**, *11*, 3217.

[20] a) T. Shimizu, M. Masuda, H. Minamikawa, *Chem. Rev.* **2005**, *105*, 1401; b) D. A. Frankel, D. F. O'Brien, *J. Am. Chem. Soc.* **1994**, *116*, 10057.

[21] W. Barthlott, C. Neinhuis, *Planta* **1997**, *202*, 1.

[22] R. N. Wenzel, *Ind. Eng. Chem.* **1936**, *28*, 988.

[23] A. B. D. Cassie, S. Baxter, *Trans. Faraday Soc.* **1944**, *40*, 546.

[24] M. Nosonovsky, *J. Chem. Phys.* **2007**, *126*, 224701.

[25] J. Shieh, F. J. Hou, Y. C. Chen, H. M. Chen, S. P. Yang, C. C. Cheng, H. L. Chen, *Adv. Mater.* **2010**, *22*, 597.

[26] V. Zorba, E. Stratakis, M. Barberoglou, E. Spanakis, P. Tzanetakis, S. H. Anastasiadis, C. Fotakis, *Adv. Mater.* **2008**, *20*, 4049.

[27] J. Wang, Y. Shen, S. Kessel, P. Fernandes, K. Yoshida, S. Yagai, D. G. Kurth, H. M. hwald, T. Nakanishi, *Angew. Chem.* **2009**, *121*, 2200; *Angew. Chem. Int. Ed.* **2009**, *48*, 2166.
[28] L. Wang, Y. Zhou, J. Yan, J. Wang, J. Pei, Y. Cao, *Langmuir* **2009**, *25*, 1306.
[29] Y. F. Shen, J. B. Wang, U. Kuhlmann, P. Hildebrandt, K. Ariga, H. Möhwald, D. G. Kurth, T. Nakanishi, *Chem. Eur. J.* **2009**, *15*, 2763.

Received: February 8, 2010
Published online: May 12, 2010

